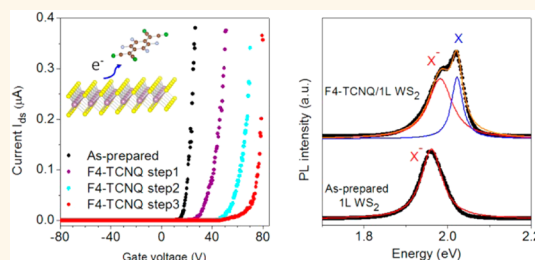


# Chemically Driven Tunable Light Emission of Charged and Neutral Excitons in Monolayer WS<sub>2</sub>

Namphung Peimyoo,<sup>†</sup> Weihuang Yang,<sup>†</sup> Jingzhi Shang,<sup>†</sup> Xiaonan Shen,<sup>†</sup> Yanlong Wang,<sup>†</sup> and Ting Yu<sup>\*†,‡,§</sup>

<sup>†</sup>Division of Physics and Applied Physics, School of Physical and Mathematical Sciences, Nanyang Technological University, Singapore 637371, <sup>‡</sup>Department of Physics, Faculty of Science, National University of Singapore, Singapore 117542, and <sup>§</sup>Graphene Research Centre, National University of Singapore, 2 Science Drive 3, Singapore 117542

**ABSTRACT** Monolayer (1L) semiconducting transition metal dichalcogenides (TMDs) possess remarkable physical and optical properties, promising for a wide range of applications from nanoelectronics to optoelectronics such as light-emitting and sensing devices. Here we report how the molecular adsorption can modulate the light emission and electrical properties of 1L WS<sub>2</sub>. The dependences of trion and exciton emission on chemical doping are investigated in 1L WS<sub>2</sub> by microphotoluminescence ( $\mu$ PL) measurements, where different responses are observed and simulated theoretically. The total PL is strongly enhanced when electron-withdrawing molecules adsorb on 1L WS<sub>2</sub>, which is attributed to the increase of the exciton formation due to charge transfer. The electrical transport measurements of a 1L WS<sub>2</sub> field effect transistor elucidate the effect of the adsorbates on the conductivity, which give evidence for charge transfer between molecules and 1L WS<sub>2</sub>. These findings open up many opportunities to manipulate the electrical and optical properties of two-dimensional TMDs, which are particularly important for developing optoelectronic devices for chemical and biochemical sensing applications.



**KEYWORDS:** tungsten disulfide · photoluminescence · exciton · trion · chemical doping · charge transfer

Layer structures of transition metal dichalcogenides (TMDs) have received considerable research interest due to their striking optical and electrical properties,<sup>1–3</sup> especially semiconducting WS<sub>2</sub>, WSe<sub>2</sub>, MoS<sub>2</sub>, and MoSe<sub>2</sub> layers. Their bulk crystals are indirect band gap semiconductors, while monolayers own direct band gaps corresponding to the visible to near-infrared photon energies,<sup>1</sup> making them more suitable than graphene for light-emitting and functional transistor applications. Recently, those semiconducting TMDs have been explored for optoelectronics such as light-emitting diodes,<sup>4–7</sup> photodetectors,<sup>8</sup> and solar cells.<sup>4</sup> Furthermore, unique symmetry and strong spin–orbital coupling enable these TMD layers to serve as a new platform for valleytronic research.<sup>9–11</sup>

The optical response of 1L TMDs is dominated by excitonic transitions: A and B excitons as observed in the optical absorption and emission spectra,<sup>12–14</sup> originating from the splitting of the valence band maximum at the K (K') point due to the large

spin–orbital interactions. The large exciton binding energies in 1L TMDs have been predicted to be 0.5–1 eV.<sup>15–17</sup> In 1L WS<sub>2</sub>, a binding energy as high as 0.5–0.7 eV has recently been extracted by temperature-dependent photoluminescence and two-photon absorption measurements.<sup>14,18</sup> It is also known that the concentrations of the negatively (X<sup>−</sup>) or positively (X<sup>+</sup>) charged excitons (so-called trions) and neutral excitons (X) in semiconducting quantum wells and quantum dots can be modulated by applying gate voltage,<sup>19</sup> chemical doping,<sup>20</sup> or laser excitation.<sup>21–23</sup> Recently, electrical doping measurements of 1L MoSe<sub>2</sub><sup>24</sup> and WSe<sub>2</sub><sup>25</sup> have shown the tunability of the excitonic species among X<sup>−</sup>, X, and X<sup>+</sup>, and electrically tunable emission between X<sup>−</sup> and X components has been observed in MoS<sub>2</sub> and WS<sub>2</sub>.<sup>18,26</sup> It is also worth noting that chemical doping *via* the absorption of gases and organic molecules has become a promising approach to tune charge carriers in graphene<sup>27,28</sup> and some TMDs.<sup>29,30</sup> By contrast, controlling the excitonic species

\* Address correspondence to yuting@ntu.edu.sg.

Received for review July 29, 2014 and accepted October 15, 2014.

Published online October 15, 2014  
10.1021/nn504196n

© 2014 American Chemical Society

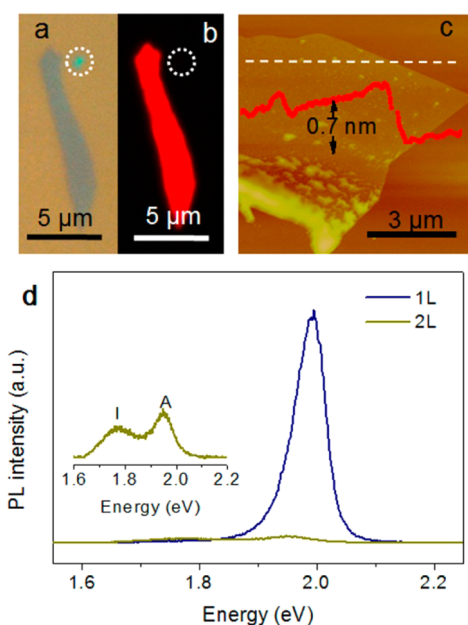


**Figure 1.** Characterization of WS<sub>2</sub> flakes. Optical microscope image of WS<sub>2</sub> flakes (a) and the corresponding fluorescence image (b), where the thick WS<sub>2</sub> flake is circled. (c) Atomic force microscope (AFM) image of a WS<sub>2</sub> flake. Inset is the AFM height profile along the dashed line. (d) Photoluminescence (PL) spectra of 1L and bilayer (2L) WS<sub>2</sub> excited by a 532 nm laser. Inset: Enlarged spectrum of a 2L presenting an indirect band gap labeled as I.

in semiconducting 1L WS<sub>2</sub> *via* chemical doping is still less explored now. Particularly, H<sub>2</sub>O molecules commonly exist in fabrication processes and operation environments of most semiconductor devices. In view of the very promising prospects of 1L WS<sub>2</sub> for light-emitting device applications, studying the influence of H<sub>2</sub>O on the light emission is very meaningful, while it has not received enough attention until now.

In this work, we demonstrate the tunability of charged and neutral excitons in 1L WS<sub>2</sub> *via* chemical doping (F<sub>4</sub>TCNQ and H<sub>2</sub>O molecules) as characterized by micro-photoluminescence (PL) spectroscopy. The electrical transport data suggest that the exfoliated 1L WS<sub>2</sub> is a naturally n-type semiconductor and clearly delineates that the electron concentration decreases when the electron-withdrawing dopant interacts with WS<sub>2</sub>. Moreover, it is found that adsorption of electron-withdrawing molecules strongly enhances the total PL by charge transfer. The changes of neutral and charged excitons are well modeled by a simplified theoretical framework. Our work demonstrates the ability of chemical doping to tune the excitonic emission species in 1L WS<sub>2</sub> and clarifies the charge transfer mechanism, which is very important for exploiting the TMDs for optoelectronic and chemical sensing applications.

## RESULTS AND DISCUSSION

WS<sub>2</sub> flakes were mechanically exfoliated from the commercial WS<sub>2</sub> crystals onto the 300 nm thick SiO<sub>2</sub> on a highly doped Si wafer. Figure 1a and b show the

optical micrograph of WS<sub>2</sub> flakes and the corresponding fluorescence image, respectively, in which striking emission is observed in the 1L region, while there is no detectable emission signal from the thicker counterpart. Hence, the fluorescence image can be used to rapidly distinguish a single layer from multilayers. The thicknesses of WS<sub>2</sub> flakes are further characterized by atomic force microscopy (AFM) and photoluminescence measurements. In Figure 1c, the AFM image shows the topological surface of a representative WS<sub>2</sub> sample, and its line scan along the white dashed line in the 1L region presents an average height of 0.7 nm.

Figure 1d shows room-temperature PL spectra of 1L and 2L WS<sub>2</sub> characterized by PL spectroscopy using 2.33 eV laser excitation, where the pronounced peak at around 1.98 eV is observed and it may contain the emission from both neutral and charged A exciton states. Note that the B exciton feature is not measurable under this laser excitation. The energy difference between the A and B excitons arises from the splitting of the valence band due to spin–orbital coupling, which is found to be ~0.4 eV for 1L and multilayer WS<sub>2</sub>.<sup>17,31</sup> The PL of 1L WS<sub>2</sub> is much more intense than that of 2L, which is strong evidence of the direct to indirect transition. The inset clarifies the spectral features for 2L, where the indirect band gap transition is denoted as I. The direct transition in 1L WS<sub>2</sub> occurs between the valence band maximum and conduction band minimum, located at the K point of the Brillouin zone according to theoretical predictions<sup>16,32</sup> and photoemission experiment.<sup>33</sup> In multilayer and bulk WS<sub>2</sub>, indirect radiative recombination exists, which involves the transition from either the K point or the midpoint along K and  $\Gamma$  of the conduction band to the  $\Gamma$  point of the valence band.<sup>32,34–36</sup>

Adsorbates and the surrounding environment can greatly tailor the electrical and optical properties of 2D semiconductors. Particularly, the effective modification of carrier concentrations in such atomically thin semiconductors may lead to very promising electronic and optoelectronic device applications. Here, a strong electron-withdrawing molecule of 2,3,5,6-tetrafluoro-7,7,8,8-tetracyanoquinodimethane (F<sub>4</sub>TCNQ) has been utilized to modulate the properties of 1L-WS<sub>2</sub>. To examine the effect of the molecular adsorption on the electrical properties of 1L WS<sub>2</sub>, a back-gated field effect transistor (FET) was fabricated. Meanwhile, the step doping technique<sup>30</sup> has been used to deposit the molecules on 1L WS<sub>2</sub>, and the electrical transport data were recorded under various doping steps. One doping step mainly includes two processes: one is the drop casting of the molecular solution on the targeted sample; the other is drying in ambient condition (see Methods). This technique is effective to tune the carrier concentration in 1L WS<sub>2</sub> as demonstrated in the following transport data. The 1L WS<sub>2</sub> device configuration is schematically shown in Figure 2a. Figure 2b is an

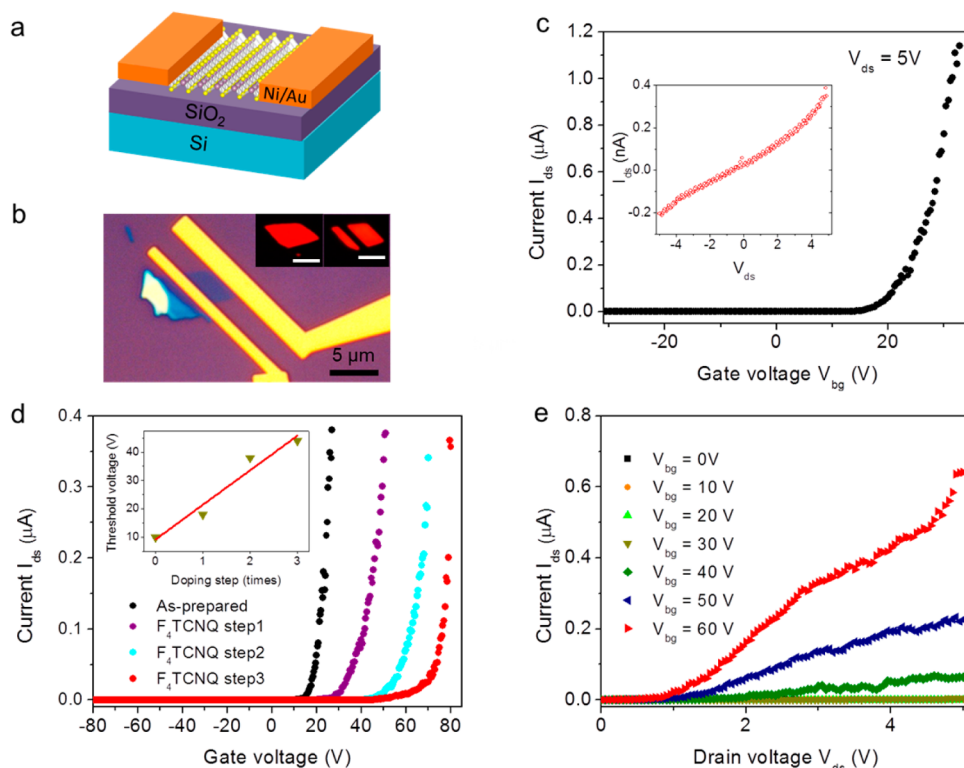


**Figure 2.** Electrical transport characteristics of 1L WS<sub>2</sub> and F<sub>4</sub>TCNQ/1L WS<sub>2</sub> at room temperature in a vacuum. (a) Schematic of the back-gated field effect transistor (FET) of 1L WS<sub>2</sub>. (b) Optical micrograph of a 1L WS<sub>2</sub> device. Inset shows fluorescence images of WS<sub>2</sub> before (left) and after (right) device fabrication, respectively. (c) Transport characteristic of the WS<sub>2</sub> FET before the F<sub>4</sub>TCNQ modification when  $V_{ds} = 5$  V. Inset: Drain current versus bias voltage ( $I_{ds}-V_{ds}$ ) curve acquired at  $V_{bg} = 0$  V. (d)  $I_{ds}-V_{bg}$  curves under  $V_{ds} = 5$  V of the as-prepared sample and after various F<sub>4</sub>TCNQ doping steps. Inset: Threshold voltage as a function of doping step. (e)  $I_{ds}-V_{ds}$  curves of F<sub>4</sub>TCNQ/1L WS<sub>2</sub> after doping step 3 recorded for different  $V_{bg}$  values.

optical image of the 1L WS<sub>2</sub> FET device, fabricated by standard electron-beam lithography. Insets of Figure 2b are fluorescence images of 1L WS<sub>2</sub> before and after device fabrication, which indicate that the intense emission can be preserved after the FET fabrication. The electrical transport characteristic of as-exfoliated 1L WS<sub>2</sub> has been measured at the bias voltage  $V_{ds}$  of 5 V under vacuum conditions, which shows the n-type behavior (Figure 2c). The native n-type doping in 1L WS<sub>2</sub> is similar to 1L MoS<sub>2</sub>,<sup>26,37</sup> which probably arises from the structural defects and/or substrate effects. At the bias voltage  $V_{ds} = 5$  V, the on-off current ratio of our device is approximately  $10^5$ . The inset of Figure 2c is the typical output ( $I_{ds}-V_{ds}$ ) characteristic of the as-exfoliated WS<sub>2</sub> FET acquired at  $V_{bg} = 0$  V. We can estimate the carrier mobility from Figure 2c using the equation  $\mu = [dI_{ds}/dV_{bg}] \times [L/WC_gV_{ds}]$ , where  $L$  and  $W$  are channel length (6.5  $\mu\text{m}$ ) and width (4  $\mu\text{m}$ ), respectively, and  $C_g$  is the gate capacitance per unit area ( $1.15 \times 10^{-4}$  F m<sup>-2</sup> for a 300 nm thick SiO<sub>2</sub> layer). The electron mobility is calculated to be  $9.5 \text{ cm}^2 \text{ V}^{-1} \text{ s}^{-1}$ , which is larger than some reported values for CVD-grown 1L WS<sub>2</sub>,<sup>38,39</sup> comparable to those obtained from the exfoliated 1L MoS<sub>2</sub> with similar device structures,<sup>40,41</sup> and smaller than that of the exfoliated 1L WS<sub>2</sub> device using the ionic liquid gate ( $44 \text{ cm}^2 \text{ V}^{-1} \text{ s}^{-1}$ ).<sup>5</sup>

Figure 2d shows representative electrical transport curves of 1L WS<sub>2</sub> before and after F<sub>4</sub>TCNQ doping at various steps. After depositing F<sub>4</sub>TCNQ for the first time, the threshold voltage shifts to the positive region by 10 V with respect to that of the as-prepared device. As the doping step increases, it significantly shifts further toward positive voltages, which suggests the effective reduction of the electron concentration in the conduction band. The threshold voltage as a function of doping step is plotted as shown in the inset of Figure 2d. Note that the effects of moisture adsorption may also cause the shift of the threshold voltage,<sup>40</sup> but it can be negligible here, as the measurements were conducted in the vacuum condition ( $\sim 10^{-5}$  mbar). The transport data elucidate that the electrons transfer from n-type 1L WS<sub>2</sub> to F<sub>4</sub>TCNQ molecules, corresponding to a neutralization process of 1L WS<sub>2</sub>. Figure 2e shows the  $I_{ds}-V_{ds}$  characteristics of 1L WS<sub>2</sub> after the third round of doping at various gate voltages. The shape of the  $I_{ds}-V_{ds}$  curve indicates the occurrence of Schottky barrier contacts in the 1L WS<sub>2</sub> FET, consistent with the recent study of a 1L MoS<sub>2</sub> device using Ti/Au contacts.<sup>42</sup> More importantly, by adjusting the back-gate voltage, the conductivity of the F<sub>4</sub>TCNQ/1L WS<sub>2</sub> can be modulated in a controllable manner.

After studying the chemical doping effect on the electrical transport properties, we further investigated

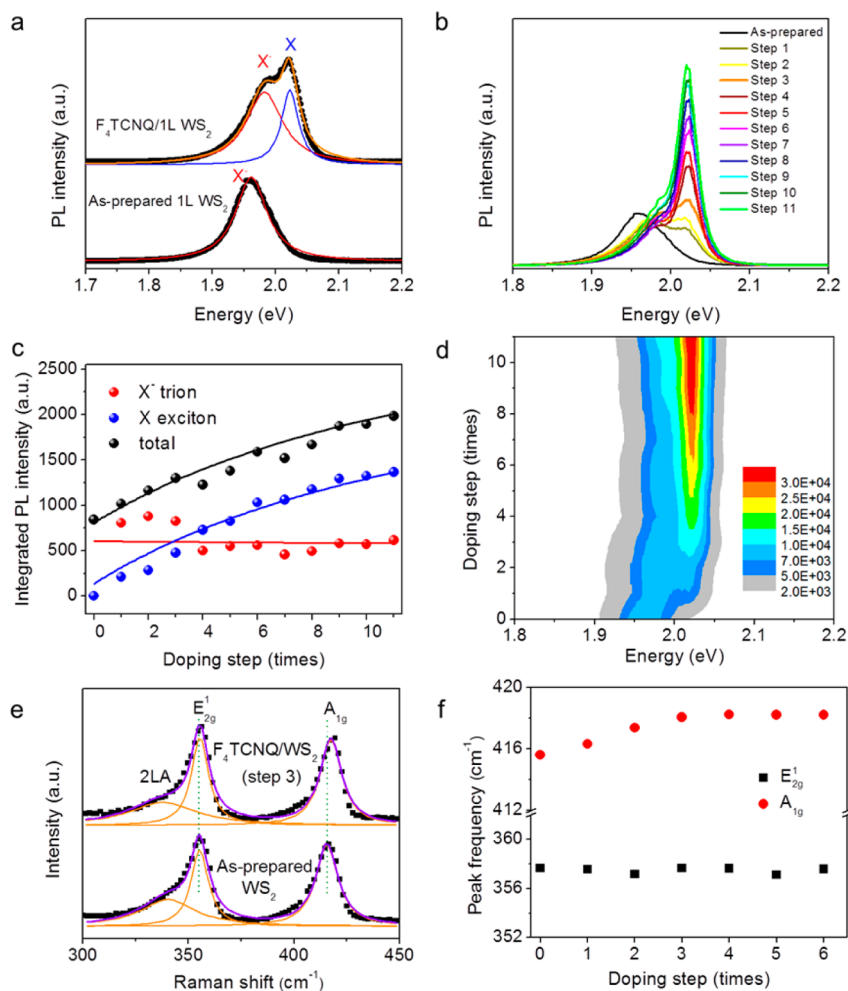


**Figure 3.** Tunable photoluminescence and Raman scattering driven by molecular adsorbates. (a) Room-temperature PL spectra of 1L WS<sub>2</sub> before and after doping with F<sub>4</sub>TCNQ. (b) PL spectra upon consecutive F<sub>4</sub>TCNQ doping. (c) Integrated PL intensities of X<sup>-</sup>, X, and the sum as a function of doping step. Solid lines are the theoretical calculation results based on the rate equation. (d) PL intensity map (in counts) as a function of doping step and photon energy. (e) Raman spectra of the 1L WS<sub>2</sub> and F<sub>4</sub>TCNQ/1L WS<sub>2</sub> under 457 nm laser excitation. (f) Peak frequencies of the E<sub>2g</sub><sup>1</sup> and A<sub>1g</sub> modes versus doping step.

the influence of molecular adsorption on the optical properties of 1L WS<sub>2</sub>. Figure 3a shows that the main emission of the as-exfoliated 1L WS<sub>2</sub> is observed at around 1.96 eV, which may be the emission from neutral and/or charged A exciton states according to previous studies.<sup>18,26</sup> After the adsorption of F<sub>4</sub>TCNQ molecules, the PL features clearly evolve into two distinct components, which can be well fitted by two Lorentzian peaks located at around 1.98 and 2.02 eV, respectively. Note that the higher energy emission in the F<sub>4</sub>TCNQ/1L WS<sub>2</sub> sample is fully absent in the PL spectrum of the as-exfoliated sample, while the lower energy peak in the F<sub>4</sub>TCNQ/1L WS<sub>2</sub> shows a very similar profile to the emission peak of the 1L WS<sub>2</sub>. Our findings of the transport measurements discussed above indicate that 1L WS<sub>2</sub> is an n-type semiconductor. Hence, the emission peak observed in the as-prepared 1L WS<sub>2</sub> sample is mainly attributed to the negatively charged trion (X<sup>-</sup>) emission, i.e., an electron-bound exciton, whereas the higher energy peak emerging after F<sub>4</sub>TCNQ adsorption is assigned to the neutral exciton

(X). In other words, the suppression of the exciton emission in the as-prepared 1L WS<sub>2</sub> is due to the unintentional n-type doping. In 1L WS<sub>2</sub>, one previous study shows that the trion emission can be observed only at low temperatures under high excitation laser powers,<sup>43</sup> while a very recent report illustrates that both the trion and exciton emission can be observed at room temperature.<sup>18</sup> The PL discrimination from these 1L WS<sub>2</sub> samples is attributed to the different electron densities from sample to sample, as demonstrated in the following. The evolution of PL spectra under successive doping (Figure 3b) shows that the X<sup>-</sup> and X emission changes differently with doping. As the doping step increases, the PL intensity of the X is remarkably enhanced, while the X<sup>-</sup> is nearly unchanged. Figure 3c shows the integrated intensity of each component and the total intensity as a function of doping step, where the details of the spectral fitting are included in the Supporting Information (see Figure S1). In the as-prepared 1L WS<sub>2</sub>, the spectral weight of the X<sup>-</sup> peak is predominant because it is rich in free

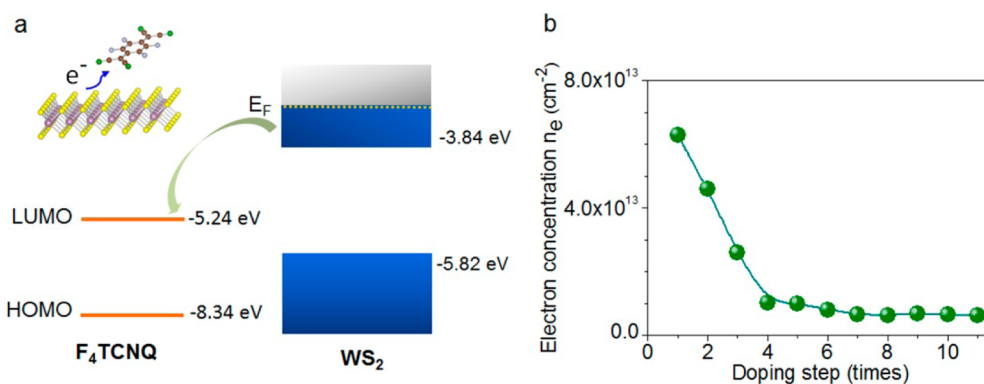


**Figure 4.** (a) Schematic of charge transfer between 1L WS<sub>2</sub> and F<sub>4</sub>TCNQ. (b) Calculated electron concentration as a function of F<sub>4</sub>TCNQ doping step.

electrons, leading to the increase of the probability of X<sup>-</sup> formation. Upon consecutive doping induced by the F<sub>4</sub>TCNQ adsorption, the integrated PL intensity of the X is monotonically enhanced, whereas the integrated intensity of X<sup>-</sup> displays a slight reduction. Above the doping step 9, the PL intensity of the X has the tendency to saturate. The electrical gating effect on PL in 1L WS<sub>2</sub> has been measured,<sup>18</sup> which supports our arguments. Theoretically, the dependences of the total intensity and the intensities of X and X<sup>-</sup> on doping have been calculated according to a rate equation and a mass-action law,<sup>23,24,30,44</sup> as denoted by the solid curves (Figure 3c), which agree fairly well with the experimental data. The details of our theoretical model are presented later.

Figure 3d shows the PL intensity map as a function of photon energy and doping step. The peak position of X<sup>-</sup> blue-shifts with the increase in F<sub>4</sub>TCNQ adsorption, while that of X remains almost unchanged with doping. The fit results are shown in Figure S2. The typical trion dissociation energy determined from the energy difference between the X and X<sup>-</sup> is found to be ~38 meV, in agreement with those obtained from the electrical gated 1L WS<sub>2</sub> device.<sup>18</sup> The trion dissociation energy decreases with the increase in deposited molecules or the decreased electron doping in 1L WS<sub>2</sub>, as shown in Figure S2, similar to the observation in electrically controlled PL for 1L MoS<sub>2</sub> and WSe<sub>2</sub>.<sup>25,26</sup> The observed trion dissociation energy is much larger than those of typical semiconductor quantum wells and quantum dots (typically in the range 1–6 meV),<sup>19,20,23,45</sup> which indicates the larger excitonic effect in such a 2D semiconductor.

Besides the doping effect discussed above, strain can also affect the PL intensity and the band gap of ultrathin TMD materials. For instance, when strain is applied in 1L MoS<sub>2</sub>, the near-band-edge emission changes.<sup>46,47</sup> Raman measurements were conducted before and after doping, in order to exclude the effect of strain on the PL change in our case. Figure 3e shows Raman spectra of the as-exfoliated 1L WS<sub>2</sub> and the F<sub>4</sub>TCNQ/1L WS<sub>2</sub>. The variations of their peak

frequencies with doping are presented in Figure 3f. It is found that the A<sub>1g</sub> mode slightly blue-shifts by 2 cm<sup>-1</sup> after the early few steps of F<sub>4</sub>TCNQ deposition, while the peak position of the E<sup>1</sup><sub>2g</sub> mode does not change. As known, in a typical 1L TMD, the out-of-plane A<sub>1g</sub> mode is susceptible to the charging effect and red-shifts with the electron doping, but the in-plane E<sup>1</sup><sub>2g</sub> mode is not affected by the doping effect, which is due to the strong electron–phonon coupling with the out-of-plane mode.<sup>48</sup> On the contrary the E<sup>1</sup><sub>2g</sub> mode has been shown to be sensitive to strain and red-shifted with increasing of both uniaxial and biaxial strain, while the A<sub>1g</sub> mode remains unchanged.<sup>47,49</sup> Thus, our observed Raman features indicate the F<sub>4</sub>TCNQ/1L WS<sub>2</sub> sample is less n-doped than that of 1L WS<sub>2</sub> due to the charge transfer during F<sub>4</sub>TCNQ adsorption; the strain effect in the F<sub>4</sub>TCNQ/1L WS<sub>2</sub> sample is negligible. These Raman studies agree well with both electrical transport and PL data above.

The PL modulation of X<sup>-</sup> and X in WS<sub>2</sub> due to F<sub>4</sub>TCNQ adsorption can be understood in terms of charge transfer, which results from the band alignments of WS<sub>2</sub> and the dopant. Figure 4a shows the calculated minimum conduction band (-3.84 eV) and maximum valence band (-5.82 eV) of WS<sub>2</sub><sup>50</sup> and the F<sub>4</sub>TCNQ HOMO (-8.34 eV) and LUMO (-5.24 eV).<sup>51</sup> Since 1L WS<sub>2</sub> is natively n-type here, the free electrons occupy the bottom of the conduction band. Due to the band offset between 1L WS<sub>2</sub> and F<sub>4</sub>TCNQ, the electrons transfer from 1L WS<sub>2</sub> to F<sub>4</sub>TCNQ, resulting in the neutralization of 1L WS<sub>2</sub> and the reduction of the probability of trion formation. The more F<sub>4</sub>TCNQ adsorption, the more electrons withdraw from the naturally n-type 1L WS<sub>2</sub>. Therefore, an enhancement in the exciton intensity in 1L WS<sub>2</sub> modified with F<sub>4</sub>TCNQ molecules is observed, while the trion spectral weight diminishes. Furthermore, we have simulated the charge transfer when a F<sub>4</sub>TCNQ molecule sits on a defined WS<sub>2</sub> unit cell. As shown in Table S1, the F<sub>4</sub>TCNQ molecule withdraws a charge of 0.1e from 1L WS<sub>2</sub>, which supports the argument above.

Our measurements indicate that the PL intensity of 1L WS<sub>2</sub> is sensitive to the adsorption of dopant molecules. In theory, the responses of the PL intensities from trion and exciton states in 1L WS<sub>2</sub> under F<sub>4</sub>TCNQ doping can be modeled by a rate equation and a mass-action law.<sup>23,24,30,44</sup> The three-level model is used as shown in the schematic (Figure S3) presenting photoexcitation (*G*), the neutral exciton recombination (*X*), the trion recombination (*X*<sup>-</sup>), and the trion formation (*F*<sub>tr</sub>). The trion formation  $F_{tr} = k_{tr}(n)N_x$ , where  $N_x$  is the population of excitons,  $k_{tr}(n)$  is the trion formation rate, and  $n$  is the doping step.<sup>30</sup> By solving the rate equation under steady-state conditions, the dependences of  $I_x$ ,  $I_{X^-}$ , and the total intensity on doping were calculated (see Supporting Information) and are shown by the blue, red, and black solid lines, respectively (Figure 3c). Our calculated results agree well with the experimental data.

The relationship among the concentrations of trions ( $N_{X^-}$ ) and excitons ( $N_x$ ) and the charge carrier density ( $n_e$ ) in semiconductors was proposed based on the law of mass action,<sup>23,24,44</sup> written as

$$\frac{N_x n_e}{N_{X^-}} = \left( \frac{4m_x m_e}{\pi \hbar^2 m_{X^-}} \right) k_B T \exp\left( -\frac{E_b}{k_B T} \right) \quad (1)$$

where  $\hbar$  is the reduced Planck's constant,  $k_B$  is the Boltzmann constant,  $T$  is the temperature,  $E_b$  is the trion binding energy,  $m_e$  is effective mass of electrons, and  $m_{X^-}$  and  $m_x$  are trion and exciton effective masses, respectively, where  $m_{X^-} = 2m_e + m_h$  and  $m_x = m_e + m_h$ . According to the theoretical calculation,<sup>17</sup>  $m_e$  and  $m_h$  are  $0.44m_0$  and  $0.45m_0$ , respectively, where  $m_0$  is the mass of a free electron.

The concentrations of trions and excitons are proportional to their PL intensities, and therefore the integrated intensity ratio of  $I_{X^-}$  to  $I_x$  can be written as<sup>30</sup>

$$\frac{I_{X^-}}{I_x} = \frac{\gamma_{tr}}{\gamma_{ex}} \left( \frac{\pi \hbar^2 m_{X^-}}{4m_x m_e} \right) \frac{n_e}{k_B T} \exp\left( \frac{E_b}{k_B T} \right) \quad (2)$$

where  $\gamma_{tr}$  and  $\gamma_{ex}$  are radiative decay rates of trions and excitons obtained from fitting parameters in rate equations, respectively. By fitting the  $I_{X^-}/I_x$  ratio in eq 2, the electron concentration in 1L WS<sub>2</sub> as a function of doping step is calculated as shown in Figure 4b. The initial electron concentration of the as-exfoliated 1L WS<sub>2</sub> can be extrapolated based on the nearly linear range in the first four doping steps, and the estimated value is  $\sim 8 \times 10^{13} \text{ cm}^{-2}$ . The electron concentration drastically drops to  $\sim 1 \times 10^{13} \text{ cm}^{-2}$  after the F<sub>4</sub>TCNQ doping step 4. After that it gradually decreases and finally reaches saturation ( $\sim 6 \times 10^{12} \text{ cm}^{-2}$ ). Our results emphasize that the physical adsorption of dopants can tune the carrier concentration in 1L WS<sub>2</sub> and strongly modulate its optical and electrical properties, which are expected to be a generic effect for other layered TMD materials as well. In particular, the sensitivity of

the excitonic species of 1L WS<sub>2</sub> to the molecular absorption can be used for optoelectronic and chemical sensing applications. Note that the as-exfoliated 1L WS<sub>2</sub> here is highly n-doped, as reflected in the suppression of the exciton peak. Similarly, the highly n-doped behavior has also been observed ( $\sim 6 \times 10^{13} \text{ cm}^{-2}$ ) in exfoliated 1L MoS<sub>2</sub>.<sup>30</sup> Such unintentional doping is probably related to the substrate condition<sup>52–54</sup> and the crystal quality.<sup>14,55</sup> In detail, one possibility is that the doping comes from trap states at the interface between WS<sub>2</sub> and the substrate. Scheuschener *et al.* have reported the n-type doping of 1L MoS<sub>2</sub> is induced by the substrate, where the trion  $X^-$  or the exciton  $X$  peak is dominant in the supported or free-standing sample, respectively.<sup>53</sup> Theoretical calculations show that the conductivity of 1L MoS<sub>2</sub> can be modulated from n- to p-type when MoS<sub>2</sub> is placed onto a SiO<sub>2</sub> substrate with the presence of different defects and impurities at the interface.<sup>54</sup> Another argument on the origin of n-type conductivity is intrinsic structural defects such as monosulfur vacancy ( $V_S$ ) and disulfur vacancy ( $V_{S_2}$ ). Intrinsic defects have been directly observed by scanning transmission electron microscopy in monolayer MoS<sub>2</sub> and WS<sub>2</sub>.<sup>55,56</sup> According to first-principles calculations based on density functional theory, some of these defects can introduce additional donor and/or acceptor levels and cause effective doping in such 1L semiconductors.<sup>55</sup>

Moreover, it has been noted that gas and H<sub>2</sub>O absorption can affect the optical and electrical properties of MoS<sub>2</sub>.<sup>29,40,57</sup> In particular, H<sub>2</sub>O is extensively used in most practical fabrication processes of electronic and optoelectronic devices and often exists in their operation atmospheres. Therefore, knowledge on the effect of H<sub>2</sub>O on PL of 1L WS<sub>2</sub> is very important, which is explored here. In our experiments, H<sub>2</sub>O was simply drop-casted onto the WS<sub>2</sub> surface, which was then covered by a glass coverslip. The PL spectra were recorded at various times to monitor their change induced by the interactions between H<sub>2</sub>O and 1L WS<sub>2</sub>. Figure 5a depicts the PL spectra of the as-prepared 1L WS<sub>2</sub> and the H<sub>2</sub>O-covered 1L WS<sub>2</sub> for 5 and 50 min, respectively. Three spectra are fitted by two Lorentzian components denoted as  $X^-$  and  $X$  to estimate the influence of H<sub>2</sub>O adsorption on the evolution of the PL line shape. The detailed analysis of the integrated intensity of each component as a function of adsorption time (Figure 5b) shows that in the as-prepared sample the  $X^-$  occupies a larger spectral weight than  $X$ . With the increase in adsorption time, the integrated PL intensity of  $X^-$  mostly does not change over time, whereas the PL intensity of  $X$  is enhanced, analogous to the effect caused by F<sub>4</sub>TCNQ as shown above. In order to further clarify the time-dependent PL behavior of H<sub>2</sub>O/1L WS<sub>2</sub>, we have performed charge transfer calculations of three kinds of configurations, as shown in Table 1. Note that the small binding energy is

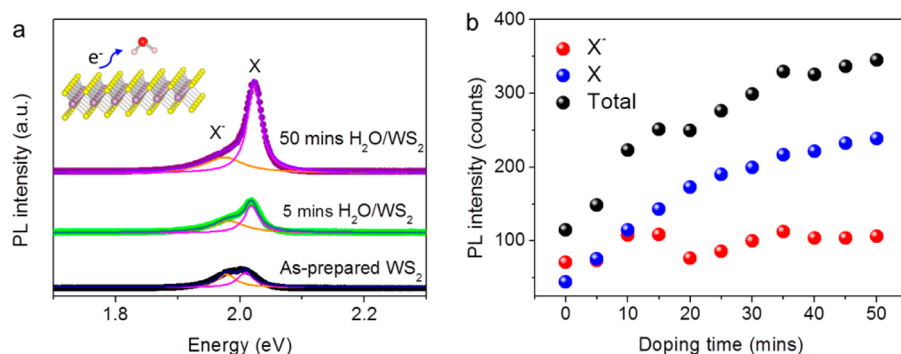


**Figure 5.** Effect of H<sub>2</sub>O adsorption on PL of 1L WS<sub>2</sub>. (a) Evolution of 1L WS<sub>2</sub> PL spectra upon H<sub>2</sub>O adsorption recorded at different times. Inset shows the charge transfer. (b) Dependence of the integrated PL intensities of trion and exciton components on the doping time.

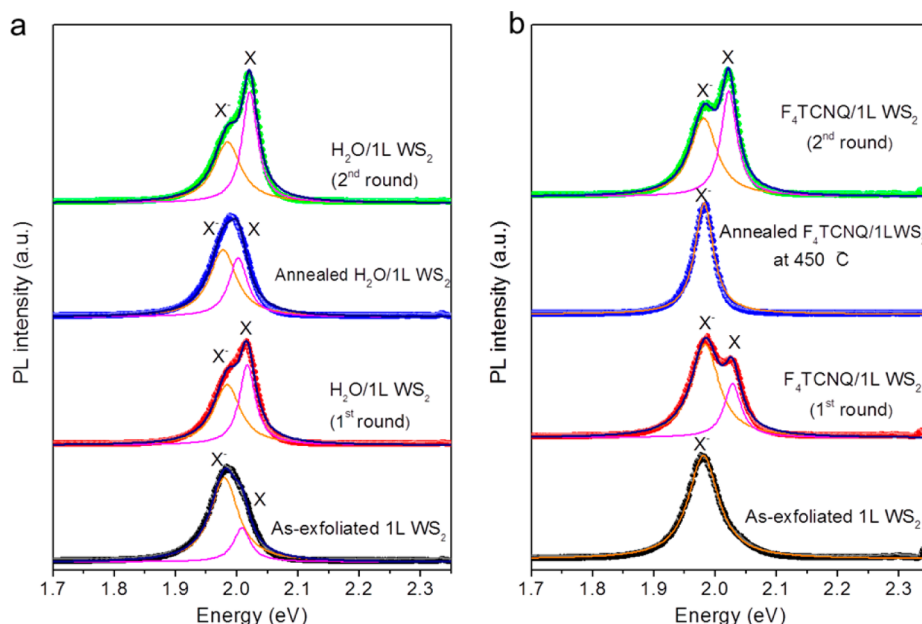


**Figure 6.** Annealing effects on the trion and exciton emission. (a) PL spectra of as-exfoliated WS<sub>2</sub>, H<sub>2</sub>O/1L WS<sub>2</sub>, and H<sub>2</sub>O/1L WS<sub>2</sub> after annealing at 150 °C in air for 20 min and redoping of the annealed sample. (b) PL spectra of as-exfoliated WS<sub>2</sub>, F<sub>4</sub>TCNQ/1L WS<sub>2</sub>, and F<sub>4</sub>TCNQ/1L WS<sub>2</sub> after annealing at 450 °C under vacuum for 20 min and F<sub>4</sub>TCNQ/1L WS<sub>2</sub> (second round).

indicative of physical adsorption, which is in the same order as the O<sub>2</sub> adsorption on 1L MoS<sub>2</sub>.<sup>58</sup> A charge of 0.09e transfers from the WS<sub>2</sub> layer to H<sub>2</sub>O when the 4 × 4 WS<sub>2</sub> unit cell adsorbs a H<sub>2</sub>O molecule. When two independent H<sub>2</sub>O molecules are adsorbed on WS<sub>2</sub>, two H<sub>2</sub>O molecules withdraw 0.11e from the WS<sub>2</sub> cell. When more H<sub>2</sub>O molecules adsorb on WS<sub>2</sub>, the coupling or interaction among these molecules becomes important. For example, when two coupled H<sub>2</sub>O molecules adsorb on WS<sub>2</sub>, these two H<sub>2</sub>O can obtain 0.16e from the WS<sub>2</sub> cell, which is more than that obtained by two independent H<sub>2</sub>O molecules. Thus, the PL change with time is attributed to more electrons transferred from 1L WS<sub>2</sub> to H<sub>2</sub>O molecules, which is caused by the increasing number of adsorbed H<sub>2</sub>O molecules and the presence of coupling among these molecules.

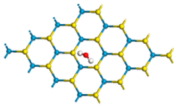
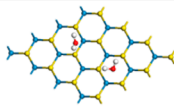
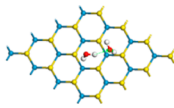
Finally, we investigate the annealing effects on the light emission from trion and exciton states of H<sub>2</sub>O/1L WS<sub>2</sub> and F<sub>4</sub>TCNQ/1L WS<sub>2</sub> samples (Figure 6a and b). It is

found that after annealing the emission spectral weight of excitons in both H<sub>2</sub>O- and F<sub>4</sub>TCNQ-attached 1L WS<sub>2</sub> substantially decreases (it vanishes for F<sub>4</sub>TCNQ-doped sample), indicating the removal of the molecular dopants. As a result, these samples become more n-doped than they do without annealing, i.e., a recovery process of n-type doping in 1L WS<sub>2</sub>. Furthermore, H<sub>2</sub>O and F<sub>4</sub>TCNQ molecules were redeposited on the same annealed samples for the second round. As seen in Figure 6, the X spectral weight increases and it is larger than that of X<sup>-</sup>. The results suggest that the evolution of the X<sup>-</sup> and X features is reversible in 1L WS<sub>2</sub> via our chemical doping and thermal annealing, which provides more flexibility for potential device applications.

## CONCLUSIONS

We have demonstrated that neutral and charged exciton emission can be tuned through adsorption of the electron-withdrawing dopants of F<sub>4</sub>TCNQ and H<sub>2</sub>O.

**TABLE 1. Calculated Binding Energies and Charge Transfer in Different H<sub>2</sub>O/WS<sub>2</sub> Configurations<sup>a</sup>**

Sample	Structure	Binding energy (eV)	Charge transfer (e) <sup>a</sup>
H <sub>2</sub> O-WS <sub>2</sub>		-0.214	0.09
2H <sub>2</sub> O-WS <sub>2</sub>		-0.362	0.11
Coupled 2H <sub>2</sub> O-WS <sub>2</sub>		-0.329	0.16

<sup>a</sup> The charge that molecules obtain from the WS<sub>2</sub> layer is analyzed by the Hirshfeld method.

The PL enhancement upon successive doping is due to the increment of exciton formation, while the formation of trions is weakened, as a consequence of the electron transfer from 1L WS<sub>2</sub> to the dopants. The electrical transport measurements confirm that the n-type semiconducting behavior is a characteristic of the used as-exfoliated samples and elucidate that the

adsorption of F<sub>4</sub>TCNQ molecules reduces the electron concentration in 1L WS<sub>2</sub>. Our studies develop a very efficient approach to control the excitonic emission species in 1L WS<sub>2</sub> and reveal the corresponding charge transfer mechanism, which is significant for optoelectronics and chemical sensing applications of 2D TMDs.

## METHODS

**Photoluminescence Spectroscopy.** WS<sub>2</sub> flakes were produced by mechanical exfoliation from commercial WS<sub>2</sub> crystals (2D Semiconductors Inc.) onto the 300 nm thick SiO<sub>2</sub> on the highly doped Si wafer. The number of layers of WS<sub>2</sub> flakes was determined by atomic force microscopy, fluorescence, and photoluminescence spectrometers. Micro-PL and Raman measurements were performed using a WITec CRM 200 system with excitation wavelengths of 532 and 457 nm. The laser power was kept as low as 40  $\mu$ W for all measurement to avoid heating and optical doping effects. In the doping-dependent PL measurements, 2,3,5,6-tetrafluoro-7,7,8,8-tetracyanoquinodimethane, known as a strong electron-withdrawing molecule, and deionized water were utilized as dopant molecules. F<sub>4</sub>TCNQ was prepared in the solvent of toluene with a concentration of 0.02  $\mu$ mol/mL. The molecular adsorption was introduced by drop-casting 10  $\mu$ L of F<sub>4</sub>TCNQ onto the WS<sub>2</sub> sample prepared on the  $\sim$ 1 cm<sup>2</sup> SiO<sub>2</sub>/Si substrate, which is recorded as one doping step. The sample was then dried in ambient conditions before collecting the PL spectra. In order to systematically study the effect of the molecule on the PL spectra, successive doping was performed by repeating the same process and controlling the same amount in the droplet for each doping step. To investigate the effect of H<sub>2</sub>O on the PL of WS<sub>2</sub>, the small droplet ( $\sim$ 10  $\mu$ L) of deionized water was placed onto the WS<sub>2</sub> sample, which was then covered by a coverslip. A series of PL spectra were recorded at different times to monitor the evolution.

**Device Fabrication.** The source and drain electrodes were made of 5/80 nm of Ni/Au by thermal evaporation and were patterned by standard electron beam lithography, followed by the lift-off process. All electrical transport measurements were measured by a Keithley 4200 SCS parameter analyzer in a vacuum system ( $\sim$ 10<sup>-5</sup> mbar) at room temperature.

**Simulation of Charge Transfer.** Monolayer WS<sub>2</sub> was constructed by 4  $\times$  4 unit cell of a 2H-WS<sub>2</sub> crystal from experimental data. The c axis of the periodic supercell was large enough (about 18.5  $\text{Å}$ )

so that the interaction between the WS<sub>2</sub> sheet and adsorbed molecule of the adjacent supercell was negligible. The geometrical optimization was carried out by use of the GGA/PW91 method with OBS correction. The pseudopotentials are norm-conserving with a 650 eV energy cutoff. The max force is 0.02, and the max stress is 0.03 GPa. All the geometrical and energy calculations were performed in a Material Studio7.0 Castep module with the GGA/PW91-OBS method.<sup>59</sup>

**Conflict of Interest:** The authors declare no competing financial interest.

**Acknowledgment.** This work is supported by the Singapore National Research Foundation under NRF RF award No. NRF-RF2010-07, MOE Tier 2 MOE2012-T2-2-049, and A\*Star SERC PSF grant 1321202101. We thank Jiwei Li for the discussion on the charge transfer mechanism.

**Supporting Information Available:** The evolution of PL spectra of 1L WS<sub>2</sub> upon sequential doping with F<sub>4</sub>TCNQ; variations of energies of the trion and the exciton peaks and the trion dissociation energy with the doping step; calculation of doping-dependent PL intensity of 1L WS<sub>2</sub> by use of the rate equations. This material is available free of charge via the Internet at <http://pubs.acs.org>.

## REFERENCES AND NOTES

- Wang, Q. H.; Kalantar-Zadeh, K.; Kis, A.; Coleman, J. N.; Strano, M. S. Electronics and Optoelectronics of Two-Dimensional Transition Metal Dichalcogenides. *Nat. Nanotechnol.* **2012**, *7*, 699–712.
- Chhowalla, M.; Shin, H. S.; Eda, G.; Li, L. J.; Loh, K. P.; Zhang, H. The Chemistry of Two-Dimensional Layered Transition Metal Dichalcogenide Nanosheets. *Nat. Chem.* **2013**, *5*, 263–275.
- Jariwala, D.; Sangwan, V. K.; Lauhon, L. J.; Marks, T. J.; Hersam, M. C. Emerging Device Applications for Semiconducting



- Two-Dimensional Transition Metal Dichalcogenides. *ACS Nano* **2014**, *8*, 1102–1120.
4. Pospischil, A.; Furchi, M. M.; Mueller, T. Solar-Energy Conversion and Light Emission in an Atomic Monolayer p-n Diode. *Nat. Nanotechnol.* **2014**, *9*, 257–261.
  5. Jo, S.; Ubrig, N.; Berger, H.; Kuzmenko, A. B.; Morpurgo, A. F. Mono- and Bilayer WS<sub>2</sub> Light-Emitting Transistors. *Nano Lett.* **2014**, *14*, 2019–2025.
  6. Ross, J. S.; Klement, P.; Jones, A. M.; Ghimire, N. J.; Yan, J.; Mandrus, D. G.; Taniguchi, T.; Watanabe, K.; Kitamura, K.; Yao, W.; *et al.* Electrically Tunable Excitonic Light-Emitting Diodes Based on Monolayer WSe<sub>2</sub> p-n Junctions. *Nat. Nanotechnol.* **2014**, *9*, 268–272.
  7. Baugher, B. W. H.; Churchill, H. O. H.; Yang, Y. F.; Jarillo-Herrero, P. Optoelectronic Devices Based on Electrically Tunable p-n Diodes in a Monolayer Dichalcogenide. *Nat. Nanotechnol.* **2014**, *9*, 262–267.
  8. Lopez-Sanchez, O.; Lembke, D.; Kayci, M.; Radenovic, A.; Kis, A. Ultrasensitive Photodetectors Based on Monolayer MoS<sub>2</sub>. *Nat. Nanotechnol.* **2013**, *8*, 497–501.
  9. Cao, T.; Wang, G.; Han, W. P.; Ye, H. Q.; Zhu, C. R.; Shi, J. R.; Niu, Q.; Tan, P. H.; Wang, E.; Liu, B. L.; *et al.* Valley-Selective Circular Dichroism of Monolayer Molybdenum Disulfide. *Nat. Commun.* **2012**, *3*, 887.
  10. Zeng, H. L.; Dai, J. F.; Yao, W.; Xiao, D.; Cui, X. D. Valley Polarization in MoS<sub>2</sub> Monolayers by Optical Pumping. *Nat. Nanotechnol.* **2012**, *7*, 490–493.
  11. Mak, K. F.; He, K. L.; Shan, J.; Heinz, T. F. Control of Valley Polarization in Monolayer MoS<sub>2</sub> by Optical Helicity. *Nat. Nanotechnol.* **2012**, *7*, 494–498.
  12. Mak, K. F.; Lee, C.; Hone, J.; Shan, J.; Heinz, T. F. Atomically Thin MoS<sub>2</sub>: A New Direct-Gap Semiconductor. *Phys. Rev. Lett.* **2010**, *105*, 136805.
  13. Zhao, W. J.; Ghorannevis, Z.; Chu, L. Q.; Toh, M. L.; Kloc, C.; Tan, P. H.; Eda, G. Evolution of Electronic Structure in Atomically Thin Sheets of WS<sub>2</sub> and WSe<sub>2</sub>. *ACS Nano* **2013**, *7*, 791–797.
  14. Peimyoo, N.; Shang, J. Z.; Cong, C. X.; Shen, X. N.; Wu, X. Y.; Yeow, E. K. L.; Yu, T. Nonblinking, Intense Two-Dimensional Light Emitter: Mono Layer WS<sub>2</sub> Triangles. *ACS Nano* **2013**, *7*, 10985–10994.
  15. Cheiwchanamangij, T.; Lambrecht, W. R. L. Quasiparticle Band Structure Calculation of Monolayer, Bilayer, and Bulk MoS<sub>2</sub>. *Phys. Rev. B* **2012**, *85*, 205302.
  16. Shi, H. L.; Pan, H.; Zhang, Y. W.; Yakobson, B. I. Quasiparticle Band Structures and Optical Properties of Strained Monolayer MoS<sub>2</sub> and WS<sub>2</sub>. *Phys. Rev. B* **2013**, *87*, 155304.
  17. Ramasubramaniam, A. Large Excitonic Effects in Monolayers of Molybdenum and Tungsten Dichalcogenides. *Phys. Rev. B* **2012**, *86*, 115409.
  18. Zhu, B. R.; Chen, X.; Cui, X. D. Exciton Binding Energy of Monolayer WS<sub>2</sub>. 2014, arXiv: condense matter/1403.5108v2. arXiv.org e-Print arXiv. <http://arxiv.org/abs/1403.5108v2> (accessed Jun 8, 2014).
  19. Finkelstein, G.; Shtrikman, H.; Bar-Joseph, I. I. Optical Spectroscopy of a Two-Dimensional Electron Gas near the Metal-Insulator Transition. *Phys. Rev. Lett.* **1995**, *74*, 976–979.
  20. Huard, V. V.; Cox, R. T.; Saminadayar, K.; Arnoult, A.; Tatarenko, S. Bound States in Optical Absorption of Semiconductor Quantum Wells Containing a Two-Dimensional Electron Gas. *Phys. Rev. Lett.* **2000**, *84*, 187–190.
  21. Glasberg, S.; Finkelstein, G.; Shtrikman, H.; Bar-Joseph, I. Comparative Study of the Negatively and Positively Charged Excitons in GaAs Quantum Wells. *Phys. Rev. B* **1999**, *59*, 10425.
  22. Shields, A. J.; Osborne, J. L.; Simmons, M. Y.; Pepper, M.; Ritchie, D. A. Magneto-Optical Spectroscopy of Positively Charged Excitons in GaAs Quantum Wells. *Phys. Rev. B* **1995**, *52*, 5523.
  23. Siviniant, J.; Scalbert, D.; Kavokin, A. V.; Coquillat, D.; Lascaray, J. P. Chemical Equilibrium between Excitons, Electrons, and Negatively Charged Excitons in Semiconductor Quantum Wells. *Phys. Rev. B* **1999**, *59*, 1602.
  24. Ross, J. S.; Wu, S. F.; Yu, H. Y.; Ghimire, N. J.; Jones, A. M.; Aivazian, G.; Yan, J. Q.; Mandrus, D. G.; Xiao, D.; Yao, W.; *et al.* Electrical Control of Neutral and Charged Excitons in a Monolayer Semiconductor. *Nat. Commun.* **2013**, *4*, 1474.
  25. Jones, A. M.; Yu, H. Y.; Ghimire, N. J.; Wu, S. F.; Aivazian, G.; Ross, J. S.; Zhao, B.; Yan, J. Q.; Mandrus, D. G.; Xiao, D.; *et al.* Optical Generation of Excitonic Valley Coherence in Monolayer WSe<sub>2</sub>. *Nat. Nanotechnol.* **2013**, *8*, 634–638.
  26. Mak, K. F.; He, K. L.; Lee, C.; Lee, G. H.; Hone, J.; Heinz, T. F.; Shan, J. Tightly Bound Trions in Monolayer MoS<sub>2</sub>. *Nat. Mater.* **2013**, *12*, 207–211.
  27. Peimyoo, N.; Yu, T.; Shang, J. Z.; Cong, C. X.; Yang, H. P. Thickness-Dependent Azobenzene Doping in Mono- and Few-Layer Graphene. *Carbon* **2012**, *50*, 201–208.
  28. Peimyoo, N.; Li, J. W.; Shang, J. Z.; Shen, X. N.; Qiu, C. Y.; Xie, L. H.; Huang, W.; Yu, T. Photocontrolled Molecular Structural Transition and Doping in Graphene. *ACS Nano* **2012**, *6*, 8878–8886.
  29. Tongay, S.; Zhou, J.; Ataca, C.; Liu, J.; Kang, J. S.; Matthews, T. S.; You, L.; Li, J. B.; Grossman, J. C.; Wu, J. Q. Broad-Range Modulation of Light Emission in Two-Dimensional Semiconductors by Molecular Physisorption Gating. *Nano Lett.* **2013**, *13*, 2831–2836.
  30. Mouri, S.; Miyauchi, Y.; Matsuda, K. Tunable Photoluminescence of Monolayer MoS<sub>2</sub> via Chemical Doping. *Nano Lett.* **2013**, *13*, 5944–5948.
  31. Zeng, H. L.; Liu, G. B.; Dai, J. F.; Yan, Y. J.; Zhu, B. R.; He, R. C.; Xie, L.; Xu, S. J.; Chen, X. H.; Yao, W.; *et al.* Optical Signature of Symmetry Variations and Spin-Valley Coupling in Atomically Thin Tungsten Dichalcogenides. *Sci. Rep.* **2013**, *3*, 1608.
  32. Kuc, A.; Zibouche, N.; Heine, T. Influence of Quantum Confinement on the Electronic Structure of the Transition Metal Sulfide TS<sub>2</sub>. *Phys. Rev. B* **2011**, *83*, 245213.
  33. Klein, A.; Tiefenbacher, S.; Eyert, V.; Pettenkofer, C.; Jaegermann, W. Electronic Band Structure of Single-Crystal and Single-Layer WS<sub>2</sub>: Influence of Interlayer van der Waals Interactions. *Phys. Rev. B* **2001**, *64*, 205416.
  34. Zhao, W. J.; Ribeiro, R. M.; Toh, M. L.; Carvalho, A.; Kloc, C.; Neto, A. H. C.; Eda, G. Origin of Indirect Optical Transitions in Few-Layer MoS<sub>2</sub>, WS<sub>2</sub>, and WSe<sub>2</sub>. *Nano Lett.* **2013**, *13*, 5627–5634.
  35. Ramasubramaniam, A.; Naveh, D.; Towe, E. Tunable Band Gaps in Bilayer Transition-Metal Dichalcogenides. *Phys. Rev. B* **2011**, *84*, 205325.
  36. Yun, W. S.; Han, S. W.; Hong, S. C.; Kim, I. G.; Lee, J. D. Thickness and Strain Effects on Electronic Structures of Transition Metal Dichalcogenides: 2H-MX<sub>2</sub> Semiconductors (M = Mo, W; X = S, Se, Te). *Phys. Rev. B* **2012**, *85*, 33305.
  37. Radisavljevic, B.; Radenovic, A.; Brivio, J.; Giacometti, V.; Kis, A. Single-Layer MoS<sub>2</sub> Transistors. *Nat. Nanotechnol.* **2011**, *6*, 147–150.
  38. Zhang, Y.; Zhang, Y. F.; Ji, Q. Q.; Ju, J.; Yuan, H. T.; Shi, J. P.; Gao, T.; Ma, D. L.; Liu, M. X.; Chen, Y. B.; *et al.* Controlled Growth of High-Quality Monolayer WS<sub>2</sub> Layers on Sapphire and Imaging Its Grain Boundary. *ACS Nano* **2013**, *7*, 8963–8971.
  39. Lee, Y. H.; Yu, L. L.; Wang, H.; Fang, W. J.; Ling, X.; Shi, Y. M.; Lin, C. T.; Huang, J. K.; Chang, M. T.; Chang, C. S.; *et al.* Synthesis and Transfer of Single-Layer Transition Metal Disulfides on Diverse Surfaces. *Nano Lett.* **2013**, *13*, 1852–1857.
  40. Late, D. J.; Liu, B.; Matte, H. S. S. R.; Dravid, V. P.; Rao, C. N. R. Hysteresis in Single-Layer MoS<sub>2</sub> Field Effect Transistors. *ACS Nano* **2012**, *6*, 5635–5641.
  41. Yin, Z. Y.; Li, H.; Li, H.; Jiang, L.; Shi, Y. M.; Sun, Y. H.; Lu, G.; Zhang, Q.; Chen, X. D.; Zhang, H. Single-Layer MoS<sub>2</sub> Phototransistors. *ACS Nano* **2012**, *6*, 74–80.
  42. Liu, B.; Chen, L.; Liu, G.; Abbas, A. N.; Fathi, M.; Zhou, C. High-Performance Chemical Sensing Using Schottky-Contacted Chemical Vapor Deposition Grown Monolayer MoS<sub>2</sub> Transistors. *ACS Nano* **2014**, *8*, 5304–5314.
  43. Mitioglu, A. A.; Plochocka, P.; Jadcak, J. N.; Escoffier, W.; Rikken, G. L. J. A.; Kulyuk, L.; Maude, D. K. Optical Manipulation of the Exciton Charge State in Single-Layer Tungsten Disulfide. *Phys. Rev. B* **2013**, *88*, 245403.
  44. Vercik, A.; Gobato, Y. G.; Brasil, M. J. S. P. Thermal Equilibrium Governing the Formation of Negatively Charged

- Excitons in Resonant Tunneling Diodes. *J. Appl. Phys.* **2002**, *92*, 1888–1892.
45. Warburton, R. J.; Schaflein, C.; Haft, D.; Bickel, F.; Lorke, A.; Karrai, K.; Garcia, J. M.; Schoenfeld, W.; Petroff, P. M. Optical Emission from a Charge-Tunable Quantum Ring. *Nature* **2000**, *405*, 926–929.
  46. Castellanos-Gomez, A.; Roldan, R.; Cappelluti, E.; Buscema, M.; Guinea, F.; van der Zant, H. S. J.; Steele, G. A. Local Strain Engineering in Atomically Thin MoS<sub>2</sub>. *Nano Lett.* **2013**, *13*, 5361–5366.
  47. Wang, Y. L.; Cong, C. X.; Qiu, C. Y.; Yu, T. Raman Spectroscopy Study of Lattice Vibration and Crystallographic Orientation of Monolayer MoS<sub>2</sub> under Uniaxial Strain. *Small* **2013**, *9*, 2857–2861.
  48. Chakraborty, B.; Bera, A.; Muthu, D. V. S.; Bhowmick, S.; Waghmare, U. V.; Sood, A. K. Symmetry-Dependent Phonon Renormalization in Monolayer MoS<sub>2</sub> Transistor. *Phys. Rev. B* **2012**, *85*, 161403.
  49. Horzum, S.; Sahin, H.; Cahangirov, S.; Cudazzo, P.; Rubio, A.; Serin, T.; Peeters, F. M. Phonon Softening and Direct to Indirect Band Gap Crossover in Strained Single-Layer MoSe<sub>2</sub>. *Phys. Rev. B* **2013**, *87*, 125415.
  50. Kang, J.; Tongay, S.; Zhou, J.; Li, J. B.; Wu, J. Q. Band Offsets and Heterostructures of Two-Dimensional Semiconductors. *Appl. Phys. Lett.* **2013**, *102*, 12111.
  51. Gao, W. Y.; Kahn, A. Controlled p-Doping of Zinc Phthalocyanine by Coevaporation with Tetrafluorotetracyanoquinodimethane: A Direct and Inverse Photoemission Study. *Appl. Phys. Lett.* **2001**, *79*, 4040.
  52. Sercombe, D.; Schwarz, S.; Del Pozo-Zamudio, O.; Liu, F.; Robinson, B. J.; Chekhovich, E. A.; Tartakovskii, I. I.; Kolosov, O.; Tartakovskii, A. I. Optical Investigation of the Natural Electron Doping in Thin MoS<sub>2</sub> Films Deposited on Dielectric Substrates. *Sci. Rep.* **2013**, *3*, 3489.
  53. Scheuschner, N.; Ochedowski, O.; Kaulitz, A. M.; Gillen, R.; Schleberger, M.; Maultzsch, J. Photoluminescence of Free-standing Single- and Few-Layer MoS<sub>2</sub>. *Phys. Rev. B* **2014**, *89*, 125406.
  54. Dolui, K.; Rungger, I.; Sanvito, S. Origin of the n-Type and p-Type Conductivity of MoS<sub>2</sub> Monolayers on a SiO<sub>2</sub> Substrate. *Phys. Rev. B* **2013**, *87*, 165402.
  55. Zhou, W.; Zou, X. L.; Najmaei, S.; Liu, Z.; Shi, Y. M.; Kong, J.; Lou, J.; Ajayan, P. M.; Yakobson, B. I.; Idrobo, J. C. Intrinsic Structural Defects in Monolayer Molybdenum Disulfide. *Nano Lett.* **2013**, *13*, 2615–2622.
  56. Elias, A. L.; Perea-Lopez, N.; Castro-Beltran, A.; Berkdemir, A.; Lv, R. T.; Feng, S. M.; Long, A. D.; Hayashi, T.; Kim, Y. A.; Endo, M.; *et al.* Controlled Synthesis and Transfer of Large-Area WS<sub>2</sub> Sheets: From Single Layer to Few Layers. *ACS Nano* **2013**, *7*, 5235–5242.
  57. Sun, L. F.; Hu, H. L.; Zhan, D.; Yan, J. X.; Liu, L.; Teguh, J. S.; Yeow, E. K. L.; Lee, P. S.; Shen, Z. X. Plasma Modified MoS<sub>2</sub> Nanoflakes for Surface Enhanced Raman Scattering. *Small* **2014**, *10*, 1090–1095.
  58. Nan, H. Y.; Wang, Z. L.; Wang, W. H.; Liang, Z.; Lu, Y.; Chen, Q.; He, D. W.; Tan, P. H.; Miao, F.; Wang, X. R.; *et al.* Strong Photoluminescence Enhancement of MoS<sub>2</sub> through Defect Engineering and Oxygen Bonding. *ACS Nano* **2014**, *8*, 5738–5745.
  59. Ortmann, F.; Bechstedt, F.; Schmidt, W. G. Semiempirical van der Waals Correction to the Density Functional Description of Solids and Molecular Structures. *Phys. Rev. B* **2006**, *73*, 205101.